Mon. Not. R. Astron. Soc. **357,** 1219–1230 (2005) doi:10.1111/j.1365-2966.2005.08718.x

Revealing the nature of double-periodic blue variables in the Magellanic Clouds

R. E. Mennickent,[1★] L. Cidale,[2] M. Díaz,[3] G. Pietrzyński,[1,4] W. Gieren[1] and B. Sabogal[1]

[1]*Departamento de Física, Facultad de Ciencias Físicas y Matemáticas, Universidad de Concepción, Casilla 160-C, Concepción, Chile*
[2]*Facultad de Ciencias Astronómicas y Geofísicas, Univ. Nacional de La Plata, Paseo del Bosque S/N, 1900 CGA, La Plata, Argentina*
[3]*Instituto de Astronomía, Geofísica e Ciências Atmosféricas, Universidade de São Paulo, CP 3386, 01060-970 São Paulo, Brazil*
[4]*Warsaw University Observatory, AL. Ujazdowskie 4, 00-478 Warszawa, Poland*

Accepted 2004 December 6. Received 2004 November 18; in original form 2004 August 18

ABSTRACT

We present the first spectroscopic data for a sample of the recently discovered blue double-periodic variables in the Magellanic Clouds. The optical spectrum of these objects is dominated by Balmer and helium absorption lines and a continuum with a blue or sometimes flat slope. Spectral classification yields B spectral types and luminosity classes mostly of type III. However, the Hβ absorption line is weaker than expected for the spectral classification in most objects. For two objects, OGLE 05060009-6855025 and OGLE 05195898-6917013 we obtained time-resolved spectroscopy, finding radial velocity variations consistent with binarity. Phasing the short-term photometric variability of these two systems with their spectroscopic ephemeris, we find that they can be interpreted as ellipsoidal variations of the brighter component in a close binary system. From the analysis of their short-term light curves and radial velocities, we estimate that the cooler component could be a B-type dwarf. Our findings support the hypothesis that double-periodic variables are close binary systems consisting of two B-type stars. The shorter periodicity in non-eclipsing systems should be the ellipsoidal variation of the more evolved component. Regarding the long-term periodicity, we find their origin in or around the brighter star, as the oscillations virtually disappear at primary eclipse. Their nature remains unknown, at the present time. We also report the discovery of three (two of them eclipsing) new double-periodic variables in the Large Magellanic Cloud. One of them shows a shortening of the long-term period by approximately 20 per cent in a couple of cycles, which coincides with an increase of the maximum oscillation brightness.

Key words: binaries: general – stars: early-type – stars: evolution – stars: mass-loss.

1 INTRODUCTION

A new type of variable star has recently been discovered in the Magellanic Clouds (Mennickent et al. 2003, hereafter M03) based on an inspection of the OGLE-II photometric data base (Zebrun et al. 2001). These authors described 30 stars showing two kinds of photometric periodic variability: a short-term cyclic variability with typical amplitude $\Delta I \sim 0.05$ mag and period P_1 between 4 and 16 d and a sinusoidal, long-term cyclic oscillation with much larger amplitude $\Delta I \sim 0.2$ mag with period P_2 in the range of 150–1000 d. M03 found that both periods seem to be coupled through the relationship $P_2 = 35.2(8)\, P_1$. In general, the short-term variability is reminiscent of those shown by Algol-type binaries, and M03 proposed that the long-term oscillation could arise in the precession of an elliptical disc fed by a Roche-lobe filling companion in a low-mass ratio Algol system.

We have started spectroscopic observations aimed at confirming the binary hypothesis and determining the spectral types of the components of the double-periodic variables (DPVs). In this paper we present our first results on visual spectroscopy of seven double-periodic variables obtained in Chile in the spring of 2003.

2 OBSERVATIONS

Spectroscopic observations were conducted at CTIO, LCO and La Silla Observatory during the year 2003. At CTIO we used the 1.5-m telescope with the Cassegrain Spectrograph and the Loral 1-K detector. Grating no 26 tilted at 15.95° and a slit width of 2 arcsec yielded a spectral range of 3500–5300 Å, and a resolution of 2 Å. Wavelength calibration functions with a typical standard deviation of 0.1 Å were obtained with around 30 He–Ar lines for

★E-mail: rmennick@stars.cfm.udec.cl

Table 1. The double-periodic variables observed spectroscopically. We give the short (P_1) and the long (P_2) photometric periods with their errors. 'Sw' and 'dw' mean a short-term light curve characterized by a single or a double wave, respectively. The eclipsing system is labelled with 'e'.

Star	$\langle V \rangle$	$\langle B-V \rangle$	$\langle V-I \rangle$	P_1 (d)	P_2 (d)	Note
OGLE 00451755-7323436	17.51	0.306	0.222	5.178(05)	171(15)	dw
OGLE 00553643-7313019	17.74	0.079	0.268	5.092(05)	176(17)	dw
OGLE 05060009-6855025	15.54	−0.019	0.081	3.849(07)	230(22)	sw
OGLE 05155332-6925581	15.58	−0.080	0.039	7.2835(16)	188(11)	e
OGLE 05195898-6917013	15.94	−0.022	0.042	2.41(10)	140(05)	sw
OGLE 05313130-7012584	15.40	0.016	0.230	9.231(21)	960(176)	sw
OGLE 05410942-7002215	17.23	0.269	0.430	6.586(09)	245(23)	dw

Table 2. Observing log. We give the number of spectra n, the exposure time in seconds, and the heliocentric Julian day for the beginning and the end of the time series (HJD range). For ESO observations, the HJD zero point is 2 452 800, and for CTIO and LCO observations it is 2 452 900.

Run	ut-date	Star	n	exp time	HJD range
ESO	03/09/03	OGLE 05410942-7002215	4	300	85.8242–85.8375
ESO	03/09/03	OGLE 05313130-7012584	3	600	85.7924–85.8072
ESO	03/09/03	OGLE 00451755-7323436	3	600	85.7022–85.7170
ESO	03/09/03	OGLE 00553643-7313019	3	600	85.7332–85.7479
ESO	03/09/03	OGLE 05060009-6855025	3	600	85.7646–85.7793
CTIO	30/10/03	OGLE 05060009-6855025	26	600	42.6160–42.8652
CTIO	30/10/03	OGLE 05155332-6925581	6	600	42.7616–42.8485
CTIO	31/10/03	OGLE 05060009-6855025	27	600	43.6367–43.8424
CTIO	01/11/03	OGLE 05060009-6855025	18	600	44.6866–44.8211
CTIO	02/11/03	OGLE 05060009-6855025	26	300	45.6633–45.8637
CTIO	02/11/03	OGLE 05195898-6917013	23	300	45.6355–45.8378
CTIO	03/11/03	OGLE 05060009-6855025	32	300	46.6248–46.8484
CTIO	03/11/03	OGLE 05195898-6917013	24	300	46.6500–46.7904
LCO	12/11/03	OGLE 05060009-6855025	8	300	55.6165–55.8362
LCO	13/11/03	OGLE 05060009-6855025	8	300	56.6317–56.8575
LCO	14/11/03	OGLE 05060009-6855025	5	300	57.6094–57.6247
LCO	15/11/03	OGLE 05060009-6855025	6	300	58.7091–58.7282
LCO	12/11/03	OGLE 05195898-6917013	10	300	55.6345–55.8599
LCO	13/11/03	OGLE 05195898-6917013	6	300	56.6509–56.6700
LCO	14/11/03	OGLE 05195898-6917013	6	300	57.6320–57.6510
LCO	15/11/03	OGLE 05195898-6917013	5	300	58.7345–58.7498

the comparison spectra. Observations of the standard star LTT 2415 were used for flux calibrations. At La Silla we used the NTT with the EMMI blue branch in medium dispersion grating mode, with grating no 4. This instrumental setup along with a 1-arcsec slit yielded a spectral range of 3500–5050 Å and a resolution of 5 Å. The standard stars EG 21 and LTT 377 were observed with a 5-arcsec slit, allowing flux calibrations for science spectra. At LCO we used the Irénée du Pont 2.5-m telescope with the Modular Spectrograph and the SiTe2 detector. The combination of grating no 600 blazed at 5000 Å, with a slit width of 1.5 arcsec, yielded a spectral range of 4000–6050 Å, and a resolution of 2.5 Å. About 60 He–Ar–Fe lines in the comparison spectra yielded wavelength calibration functions with a standard deviation of 0.2–0.3 Å. The targets are listed in Table 1 and details of the observations are given in Table 2.

3 RESULTS

Before giving the spectroscopic results we introduce three newly discovered double-periodic variables which are important for the discussion of the phenomenon in Section 4.

3.1 New double-periodic variables found in the OGLE photometric data bases

In the course of our search for Be stars in the Magellanic Clouds (Mennickent et al. 2002, hereafter M02) based on the OGLE catalogue (Zebrun et al. 2001), we have discovered three other new double-periodic variables in the Large Magellanic Cloud (LMC) which were missed by M03. They are OGLE 05052263-6852002, OGLE 05082755-6937251 and OGLE 05200407-6936391. These stars are listed in Table 3 along with their average V magnitude and colours and the result of our period-finding analysis. We find short (P_1) and long (P_2) photometric periods with values in the same range as for other double-periodic variables. The light curves for these objects are shown in Figs 1–3, revealing the long-term periodicity and the character of the short-term variability. Two stars are eclipsing binaries, OGLE 05052263-6852002 and OGLE 05200407-6936391, showing two unequal minima in the short-term light curve. From the depth of the minima we find that the cooler component has an effective temperature roughly 80 per cent the temperature of the hotter component. This is typical for the double-periodic eclipsing binaries reported by M03; in fact, analysing their

Table 3. The new double-periodic variables in the LMC. We give the short (P_1) and the long (P_2) photometric periods with their errors. Dw means double wave and e eclipsing. HJD_0 is the time for the main minimum of the short-term light curve (+2 450 000).

Star	$\langle V \rangle$	$\langle B-V \rangle$	$\langle V-I \rangle$	P_1 (d)	P_2 (d)	HJD_0	Note
OGLE 05052263-6852002	17.471	0.063	0.218	6.2968(30)	207(15)	732.0152(38)	e
OGLE 05082755-6937251	15.528	0.088	0.172	9.7676(20)	351(45)	731.0276(260)	dw
OGLE 05200407-6936391	14.976	−0.099	−0.031	10.0316(03)	270(20)	453.0145(59)	e

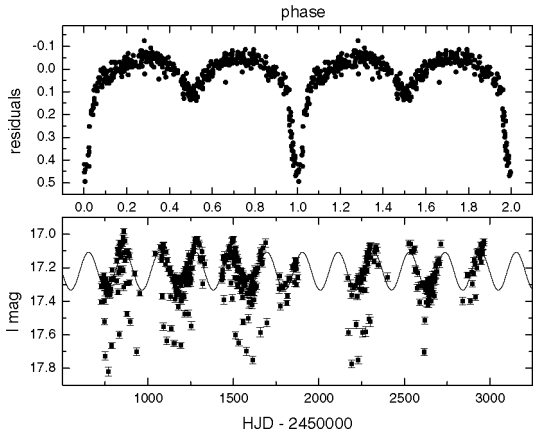

Figure 1. Long-term light curve of OGLE 05052263-6852002 and the best sinus fit (bottom) and residuals folded with the short-term period (up).

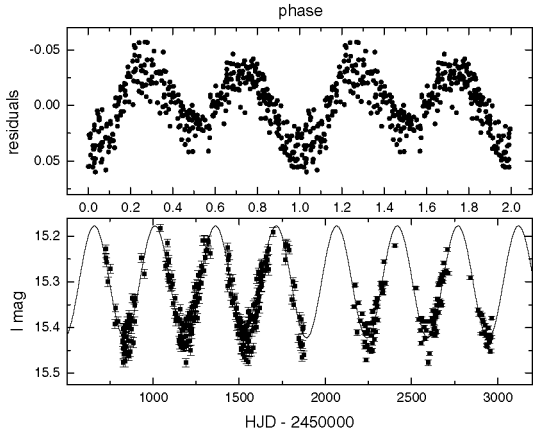

Figure 2. Long-term light curve of OGLE 05082755-6937251 along with the best sinus fit (bottom) and residuals folded with the short-term period (up).

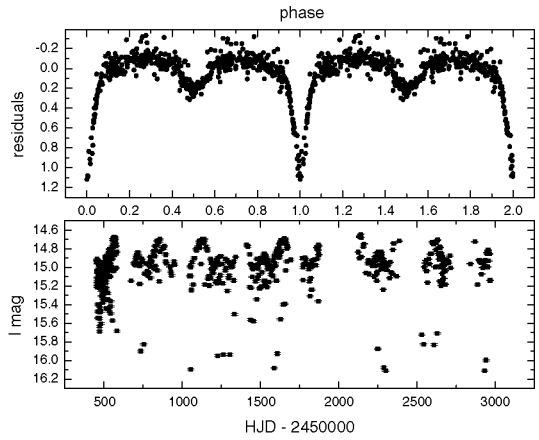

Figure 3. Long-term light curve of OGLE 05200407-6936391 (bottom). This light curve was folded with the long-term period and a fourth-order polynomial was fitted. Residuals to this polynomial are shown phased with the short-term period in the upper graph. The choice of a different pre-whitening function does not have a significant effect on our conclusions (see Section 4.2).

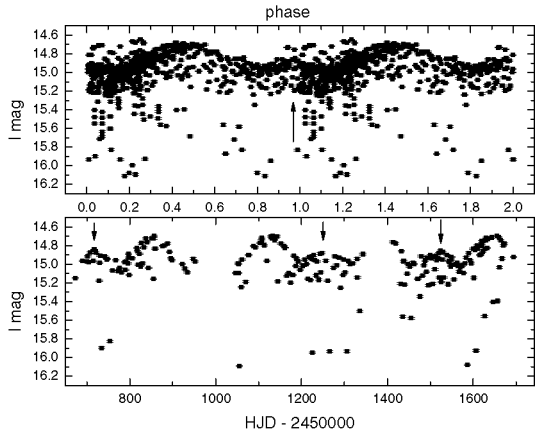

Figure 4. The bottom graph shows a zoom into the long-term light curve of OGLE 05200407-6936391. Secondary maxima are indicated with arrows. The upper graph shows the light curve folded with the long-term period of 270 d. Phase zero is HJD 2 450 453.0145. The region where the secondary maxima appear is indicated by an arrow.

light-curve minima we have found temperatures for the cooler component between 81 and 94 per cent of the temperature of the hotter component. Consistently, the same light curves reveal no significant colour modulation during the orbital cycle. In addition, we find that the short- and long-term periods of OGLE 05052263-6852002 and OGLE 05082755-6937251 closely follow the empirical relationship discovered by M03, namely $P_2 = 35.2(8)\, P_1$. The case of the eclipsing OGLE 05200407-6936391 is very interesting, as this star is the only double-periodic variable deviating to a large degree from this relationship. The predicted value 353 d, is too long compared with the observed value of 270 ± 20 d. In particular, this star presents a long-term light curve that it is not strictly sinusoidal, but it shows two maxima of different amplitude. Fig. 4 shows a zoom into the long-term light curve of this variable and the phase curve obtained folding the data with the 270-d periodicity. The anomaly around phase 1 is evident. The peculiarity of this star is confirmed in the MACHO data base; the long-term modulation changed from a period of 340 d (close to the predicted value) which was observed between HJD 2 448 800 and 2 450 000 to a period near to 270 d around HJD 2 450 500, while the maximum brightness of the modulation increased (Fig. 5). This interesting result places securely strong

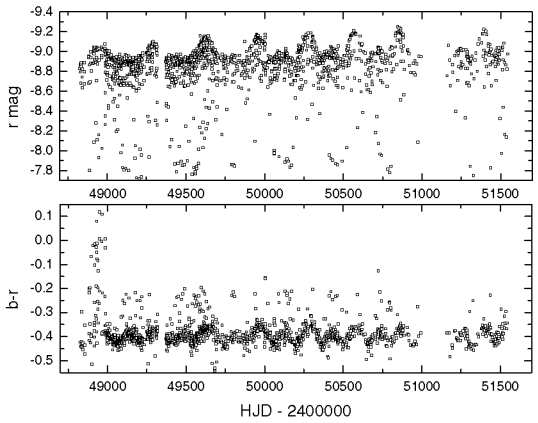

Figure 5. The long-term MACHO light curve of OGLE 05200407-6936391 showing the development of the long-term variability and the shortening of the period.

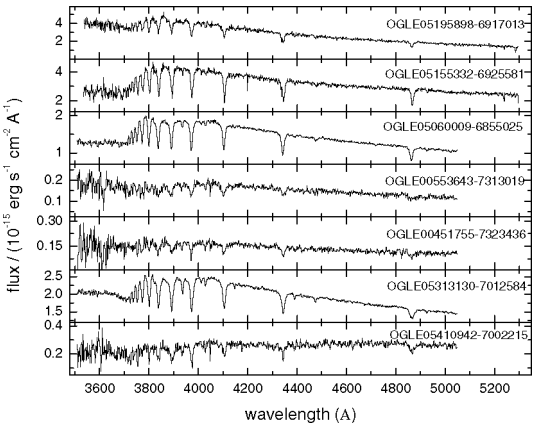

Figure 6. Average spectra for double-periodic blue variables.

constraints on the possible models aimed at explaining the long-term variability. For instance, any proposed mechanism should be able to explain: (i) the smooth development of the oscillation amplitude; (ii) the time-scale involved in the phenomenon; (iii) the fact that the period decreases while the amplitude of the oscillation increases; and (iv) the abrupt colour change just before HJD 24 490 000. The fact that the long-term variability in DPVs could be a not strictly periodic phenomenon was recently pointed out by Mennickent et al. (2004).

The large fraction of eclipsing binaries (six cases, OGLE 05171401-6936374 was probably misclassified as an eclipsing binary in M03) found in the whole sample of 33 double-periodic variables is amazing. The probability of identifying this kind of variable seems to depend on the system inclination, being larger for high-inclination systems. We suspect that some of the type 3 stars reported by M02 and not classified as double-periodic variables could be the same kind of system but seen at lower inclination. In these cases the amplitude of the short-term oscillation could be undetected only by a projection factor. This is consistent with an interpretation as ellipsoidal variations of a gravitationally distorted star in a close binary system. This view is also supported by the observations discussed in Section 3.4.

3.2 Spectroscopy of seven double-periodic variables

The average spectra of the seven double-periodic variables observed spectroscopically are shown in Fig. 6. We averaged 47 CTIO spectra for OGLE 05195898-6917013, six CTIO spectra for OGLE 05155332-6925581, four NTT spectra for OGLE 05410942-7002215 and three NTT spectra for each of the others. The relative strength of Ca II 3933 and Hϵ, along with the presence of He I 4471, suggests a B-type spectral classification for most objects. Particularly interesting is the flattening of some spectra, such as those of OGLE 05410942-7002215, OGLE 00451755-7323436 and OGLE 00553643-7313019 and the weakness of the Hβ absorption line, especially in OGLE 00451755-7323436 and OGLE 00553643-7313019, the only two stars in the Small Magellanic Cloud (SMC) in our sample.

The spectral classification of the stars observed spectroscopically was derived considering both the Barbier–Chalonge–Divan (BCD) spectrophotometric system and the measurement of the equivalent width of some selected lines (Didelon 1982). The BCD stellar classification system, was introduced by Barbier & Chalonge (1941) and Chalonge & Divan (1952). It is based on measurable quantities of the Balmer discontinuity (BD). This system is useful for stars ranging from spectral type O4 to F9 where the BD is larger than approximately 0.005 dex. In the 3500–4600 Å region two spectrophotometric parameters are defined: D in dex and λ_1, the latter is commonly presented as the difference $\lambda_1 - 3700$ Å. D is a measure of the Balmer jump at 3700 Å, which is obtained by extrapolating the Paschen continuum energy distribution in a log F_λ/B_λ versus $1/\lambda$ display (B_λ is a reference flux distribution of known temperature). λ_1 gives the mean spectral position of the BD. D is a strong indicator of the effective photospheric temperature and λ_1 is related to the photospheric log g parameter. The BCD parameters have the advantage that they are not affected either by interstellar extinction or by circumstellar absorption and/or emission. Therefore, the BCD system is also suitable for the spectral classification of objects with circumstellar material, even for those peculiar stars showing the B[e] phenomenon (Cidale, Zorec & Tringaniello 2001). From the observed (λ_1, D) BCD parameters we can determine the fundamental parameters of stars ($T_{\rm eff}$, log g, M_V, $M_{\rm bol}$) and the spectral type using the calibrations of (λ_1, D) given by Divan & Zorec (1982) and Zorec (1986). The advantages and uncertainties of determining fundamental parameters are discussed in Divan & Zorec (1982) and Zorec & Briot (1991).

The results of the BCD spectral classification are shown in Table 4. We confirm the B-type classification for all objects. Most stars are classified as giants, coinciding with their position above the main sequence (see Section 4). Only the two objects in the SMC, OGLE 00451755-7323436 and OGLE 00553643-7313019, are spectroscopically classified as dwarfs. However, these objects, along with OGLE 05410942-7002215, turned out to be very hard to classify as their spectra display either a small Balmer discontinuity or a small signal-to-noise (S/N) ratio. These objects show a very peculiar flat continuum with weak absorption lines, and their BCD classification turned out to be more uncertain.

When interpreting the flux distribution and the colour of double-periodic variables, we should consider how binarity (which is probed in Section 3.4) affects the BCD classification. We investigated the MACHO short-term light curves for the three objects showing peculiar flux distributions and find no colour variation during the orbital cycle. This is consistent with our results of Section 4, indicating dwarf-like secondaries. Hence, the peculiar flux distribution in these objects cannot be attributed to merging of stellar continuum at different temperatures. Assuming that the Balmer jump represents the

Table 4. Results of the BCD classification. We give the BCD parameters D and λ_1 along with the corresponding effective temperature, surface gravity and absolute magnitude, bolometric magnitude and spectral type. The column 'Notes' indicates if the equivalent widths of non-H I lines are consistent with the BCD classification. Cases with weak Hβ absorption are indicated.

Star	D	λ_1	$T_{\rm eff}$	log g	$M_{\rm bol}$	M_V	Sp	Notes
OGLE 00451755-7323436	0.118	52.83	23 500	3.8	−5.5	−3.2	B1IV	Yes, Hβ weak
OGLE 00553643-7313019	0.115	81.41	26 500	4.2	−5.5	−2.0	B1V	Yes, Hβ weak
OGLE 05060009-6855025	0.240	32.50	13 500	2.8	−4.2	−3.2	B5III	Doubtful, Hβ weak
OGLE 05155332-6925581	0.232	37.63	14 700	3.1	−3.7	−2.6	B5III	Yes, Hβ weak
OGLE 05195898-6917013	0.225	44.36	16 000	3.5	−3.7	−2.2	B4III	Yes, Hβ weak
OGLE 05313130-7012584	0.187	43.08	18 000	3.3	−4.3	−2.7	B3III	Doubtful, Hβ weak
OGLE 05410942-7002215	0.107	43.00	22 000	2.9	−6.5	−4.6	B0–B1 III	Doubtful

contribution of a single star, we estimate errors of ΔD between 0.01 and 0.02. The largest discrepancies correspond to spectra with a low S/N ratio. The uncertainties in ΔD yields errors between 500 and 1500 K for $T_{\rm eff}$, ∼0.5 for log g and ∼0.5 for M_V.

The spectral type of our sample stars can also be determined by measuring the line equivalent widths. Didelon (1982) showed that the equivalent width of lines such as Hβ, He I 4471.48, Mg II 4481.23, He I 4026.19, Si II 3856.02 and He I 4143.76 are indicators of spectral type and luminosity class for the B-type stars. However, the solutions in many cases are not unique, and different classifications are sometimes possible for the same set of parameters. In general, stars with spectral types either in the range B0–B2 or B4–B7 have similar He I equivalent widths (EW). This fact, along with the issue that many weak lines were measured at the limit of our instrumental resolution, yielded to consider this method as a reference, providing only a range for the possible spectral type classification. Table 5 lists our measurements of EW. These values are consistent with the spectral types derived from the BCD spectral classification.

A comparison between spectral types derived from the BCD classification and the line spectral analysis (Didelon 1982) shows in general discrepancies from 1 to 2 B subspectral types. In some cases the earliest spectral types correspond to the BCD system which is consistent with the fact that (λ_1, D) parameters are obtained from the continuum energy distribution originating in atmospheric layers deeper than those giving rise to spectral lines.

Table 5 indicates that the Hβ line is weaker than expected for the adopted spectral type in most systems (including two of the three peculiar objects). We find the same behaviour for the Hγ absorption line. We discuss the apparent filling by emission in these lines and the colour excess (see below) in Section 4.4.

A comparison of $(B-V)_0$ values computed from OGLE II photometry (assuming uniform reddening for each LMC and SMC OGLE field, Udalski et al. 1998, 1999) with $(B-V)_0$ values obtained from spectral data (using colour–temperature calibrations, Flower 1977) shows intrinsic reddening for some of the objects listed in Table 4. Such reddening could be presumably due to circumstellar emission and/or to gravity darkening of the underlying star (Slettebak 1985). The major discrepancy $\Delta(B-V)_0$, between 0.25 and 0.45, corresponds to the objects with a peculiar flat continuum and a weak Hβ line absorption, OGLE 05410942-7002215, OGLE 00451755-7323436 and OGLE 00553643-7313019. OGLE 05313130-7012584 show an intrinsic colour excess $\Delta(B-V)_0 = 0.17$ which is similar to those found for Be stars in galactic clusters (Slettebak 1985) while the rest of the objects have $\Delta(B-V)_0 < 0.08$.

3.3 Search for variability of the Hβ absorption line in OGLE 05060009-6855025 and OGLE 05195898-6917013

Equivalent widths were measured by fitting the absorption lines with a Gauss function and determining the area under the fit. These measurements were compared with those obtained by directly evaluating the integral flux under the (interpolated) linear continuum along the line full width at zero intensity. The results were consistent, but they showed a mean shift of the values obtained with the later method by +0.4 Å. For OGLE 05060009-6855025, we investigated whether or not there was some evidence for variability in the strength of the Hβ absorption line. The mean equivalent width for this line and its standard deviation was 4.3 ± 0.3, 4.4 ± 0.5 and 4.5 ± 0.3 Å for the ESO, CTIO and LCO runs, respectively, revealing that the line was stable at the level of 10 per cent during a 2-month interval. In any case, the line is much weaker than expected for a B5III star, by ≈2.8 Å. For OGLE 05195898-6917013, the corresponding figures were 4.3 ± 0.7 and 3.7 ± 0.4 Å for the CTIO and LCO runs, respectively, indicating a constancy of the line strength at the 15 per cent level and also a filling by emission by an amount similar to OGLE 05060009-6855025.

Table 5. Equivalent widths in Å. The error is <8 per cent except for Hβ < 15 per cent. In some cases the measurement was not possible due to line blending, line not visible or noisy spectrum. H$'_\beta$ indicates the theoretical value estimated from the spectral type using the models by Collins, Truax & Cranmer (1991).

Star	H$_\beta$	H$'_\beta$	He I 3819	He I 4026	He I 4144	He I 4388	He I 4471	Mg II 4481
OGLE 00451755-7323436		4.0	0.81	1.48		1.60	1.05	
OGLE 00553643-7313019		4.0	1.04		0.55	0.53	1.28	0.84
OGLE 05060009-6855025	4.40	7.0		0.53	0.21		0.52	
OGLE 05155332-6925581	5.30	7.0		0.62	0.31	0.46	0.64	0.15
OGLE 05195898-6917013	4.00	7.0		0.98		0.78	0.62	0.32
OGLE 05313130-7012584	3.94	4.8	0.66	0.68	0.31		0.65	0.31
OGLE 05410942-7002215	5.70	4.0		1.60	0.29			

3.4 Radial velocity analysis

We selected two objects, OGLE 05060009-6855025 and OGLE 05195898-6917013, for a time-resolved radial velocity (RV) study. For the time-series obtained at CTIO and LCO, we normalized the spectra, fitting the continuum with a low-order polynomial. Then we measured radial velocities by cross-correlating every spectrum with a reference spectrum, obtained by averaging the best quality spectra per run. For that the IRAF task *fxc* was used. At our resolution, the merging of spectra with different radial velocities is not a problem. The velocities of every spectrum were shifted to an absolute scale correcting for the velocities of every template. The template velocities were obtained by fitting the Balmer lines with Gauss functions and finding the central velocity. Very noisy spectra were discarded for further RV analysis, letting 145 spectra for OGLE 05060009-6855025 and 102 spectra for OGLE 05195898-6917013. Finally, the heliocentric correction was applied to each radial velocity. Results are given in Tables 6 and 7.

Our observations were too sparse to search for periodicities in our RV time series. However, we investigated whether or not the velocities were consistent with the idea that the short photometric periods reflected the orbital motion in a binary star. The result of folding the RV data set for OGLE 05060009-6855025 with its short photometric period is shown in Fig. 7. The fit is excellent when we use as a folding period twice the short photometric period. This empirical result supports, for this object, the assumption made by M03 that P_1 reflects the orbital period in a binary star, and that the single wave character of the light curve in some systems indicates that the true orbital period is twice P_1. The best sinus fit yields an ephemeris $\mathrm{HJD}_0 = 2\,452\,899.3063 \pm 0.0637$ for the time of passing through the mean from higher to lower RV. The radial velocity half-amplitude is $K = 115 \pm 6\,\mathrm{km\,s^{-1}}$ and the mean velocity is $\gamma = 290 \pm 4$ km s^{-1}. We performed the same exercise for OGLE 05195898-6917013, the short-term light curve of which also shows a single wave. The result of folding the RV data with twice P_1 is shown in Fig. 8. In this case the best sinus fit yields an ephemeris $\mathrm{HJD}_0 = 2\,452\,902.4840 \pm 0.1730$, a radial velocity half-amplitude $K = 102 \pm 27$ km s^{-1} and a mean velocity $\gamma = 355 \pm 18$ km s^{-1}. The high-γ values found in both systems are consistent with their positions in the Magellanic Clouds (Welch et al. 1991).

We analysed how the short-term photometric variability ephemeris is related to the spectroscopic ephemeris for OGLE 05060009-6855025 and OGLE 05195898-6917013. To this end, we fit the long-term light curves obtained from the OGLE data bases with sinus functions. The residuals were phased with the spectroscopic ephemeris and the results are shown in Figs 9 and 10. We find that the short-term photometric variability attains maxima and minima approximately at phases 0.25 and 0.75. The discrepancy of 0.05 cycles for OGLE 05195898-6917013 could be due to their lower precision ephemeris. The above finding is important as it reveals that the source of the ellipsoidal variations is the brighter component, the B-type star where the Hβ radial velocity was measured. The rotation of the distorted B-giant produces the short-term photometric variability, the two maxima will be equal as the system is seen broad-side on at maximum and minimum RV. However, the two minima can vary in depth, as the cusp of the first Lagrangian point could be the coolest part of the lobe (by the von-Zeipel law) and give rise to the deeper minimum. Different minima are really

Table 6. Heliocentric radial velocities (in km s^{-1}) of the Hβ absorption line for OGLE 05060009-6855025.

HJD	RV	HJD	RV	HJD	RV	HJD	RV	HJD	RV
2944.6866	290	2942.7950	359	2943.8108	395	2945.8600	198	2946.8365	25
2944.6937	326	2942.8021	365	2943.8179	413	2945.8637	240	2946.8402	154
2944.7008	381	2942.8113	370	2943.8282	422	2946.6248	37	2955.6165	115
2944.7098	408	2942.8184	378	2943.8353	393	2946.6284	272	2955.6203	169
2944.7169	321	2942.8255	358	2943.8424	364	2946.6321	224	2955.6241	170
2944.7240	350	2942.8578	371	2945.6633	227	2946.6357	235	2955.8248	148
2944.7374	350	2942.8652	383	2945.6669	194	2946.6393	245	2955.8248	143
2944.7446	249	2943.6367	325	2945.6705	297	2946.6430	200	2955.8286	190
2944.7517	409	2943.6439	375	2945.6742	275	2946.6996	263	2955.8324	180
2944.7608	347	2943.6510	383	2945.6778	285	2946.7032	189	2955.8362	176
2944.7679	398	2943.6604	371	2945.6814	200	2946.7069	224	2956.6317	276
2942.6160	421	2943.6675	397	2945.6868	288	2946.7105	216	2956.6355	244
2942.6231	404	2943.6747	358	2945.6904	321	2946.7141	258	2956.6393	275
2942.6302	361	2943.6845	348	2945.6940	257	2946.7178	233	2956.6431	273
2942.6391	413	2943.6916	391	2945.6977	328	2946.7232	161	2956.8461	242
2942.6462	389	2943.6987	399	2945.7013	325	2946.7268	157	2956.8499	293
2942.6533	419	2943.7076	414	2945.7049	276	2946.7304	133	2956.8537	313
2942.6627	415	2943.7147	388	2945.7671	376	2946.7341	231	2956.8575	275
2942.6698	441	2943.7218	407	2945.7708	443	2946.7413	246	2957.6094	346
2942.6769	436	2943.7308	445	2945.7744	406	2946.7985	213	2957.6132	384
2942.6928	394	2943.7379	446	2945.7780	283	2946.8022	235	2957.6171	348
2942.6999	430	2943.7451	406	2945.7817	258	2946.8058	187	2957.6209	332
2942.7087	399	2943.7539	393	2945.7853	438	2946.8094	239	2957.6247	341
2942.7158	373	2943.7610	341	2945.7934	206	2946.8131	170	2958.7092	338
2942.7229	422	2943.7681	422	2945.7970	194	2946.8167	200	2958.7130	429
2942.7321	416	2943.7771	392	2945.8006	284	2946.8220	216	2958.7168	418
2942.7392	402	2943.7842	433	2945.8043	265	2946.8256	168	2958.7206	351
2942.7464	433	2943.7913	401	2945.8079	232	2946.8293	253	2958.7244	419
2942.7879	369	2943.8037	413	2945.8115	337	2946.8329	128	2958.7282	352

Table 7. Heliocentric radial velocities (in km s^{-1}) of the Hβ absorption line for OGLE 05195898-6917013.

HJD	RV	HJD	RV	HJD	RV	HJD	RV	HJD	RV
2945.6391	394	2945.8378	230	2946.7795	341	2957.6358	326	2956.6509	171
2945.6428	619	2946.6500	375	2946.7832	373	2957.6396	338	2956.6548	202
2945.6464	355	2946.6536	290	2946.7868	221	2957.6434	312	2956.6586	290
2945.6500	496	2946.6572	289	2946.7904	307	2957.6472	256	2956.5803	210
2945.6537	657	2946.6609	256	2955.6345	139	2957.651	296	2956.6662	270
2945.7137	461	2946.6645	400	2955.6383	347	2958.7345	393	2956.6700	255
2945.7174	399	2946.6681	357	2955.6421	348	2958.7383	517	2957.6320	374
2945.7210	439	2946.6735	488	2955.6459	292	2958.7422	404	2957.6358	242
2945.7246	402	2946.6772	101	2955.6497	235	2958.746	566	2957.6396	330
2945.7319	485	2946.6808	303	2955.8447	229	2958.7498	291	2957.6434	320
2945.7372	405	2946.6844	361	2955.8485	109	2958.7345	385	2957.6472	315
2945.7409	383	2946.6881	224	2955.8523	272	2955.6345	293	2957.6510	349
2945.7445	371	2946.6917	469	2955.8561	276	2955.6383	352	2958.7345	486
2945.7481	438	2946.7488	135	2955.6791	321	2955.6421	384	2958.7383	422
2945.7518	486	2946.7524	219	2956.6509	269	2955.6459	210	2958.7422	421
2945.7554	384	2946.7560	359	2956.6548	247	2955.6497	191	2958.7460	476
2945.8197	716	2946.7597	413	2956.6586	285	2955.8447	168	2958.7498	396
2945.8233	480	2946.7633	455	2956.5803	282	2955.8485	169	2958.7345	485
2945.8269	401	2946.7669	358	2956.6662	243	2955.8523	297		
2945.8306	401	2946.7723	260	2956.6700	326	2955.8561	274		
2945.8342	561	2946.7759	401	2957.6320	269	2955.6791	399		

observed in the majority of the double-periodic variables, but the two cases under study, OGLE 05060009-6855025 and OGLE 05195898-6917013, show minima of roughly equal depth. This could indicate a lower inclination for these systems or an underfilling of the Roche lobe.

4 DISCUSSION

4.1 Double-periodic variables as semidetached binaries

The working hypothesis outlined by M03 suggests that these newly discovered variables are semidetached binaries experiencing a process of mass transfer. This scenario includes the existence of a gaseous disc precessing in the comoving system of rest. As we will show, this view places severe constraints on the nature of the binary components. The mean density ρ (g cm^{-3}) for a lobe-filling donor star is related to the orbital period P (d) by

$$P\rho^{1/2} = 0.1375 \left(\frac{q}{1+q}\right)^{1/2} r_{\rm L}^{-3/2} \quad (1)$$

(Eggleton 1983), where $r_{\rm L}$ is in units of the orbital separation and can be approximated, to better than 1 per cent over the whole range of mass ratios $q(M_2/M_1)$ as

$$r_{\rm L} = \frac{0.49q^{2/3}}{0.6q^{2/3} + \ln(1+q^{1/3})} \quad (2)$$

(Eggleton 1983). Hence, $P\rho^{1/2}$ is a function of q only and over the range $0.01 \leqslant q \leqslant 10$, varies by less than 20 per cent from the value 0.37. In the following, the index 2 refers to the donor star (the brighter, primary star) and 1 to the mass-gaining companion (the fainter, secondary star).

For periods between 5 and 18 d, as are observed in double-periodic variables, we found average densities of between 5×10^{-3} and 4×10^{-4} g cm^{-3}, corresponding to O-K giants or O-B supergiants (Cox 2000).

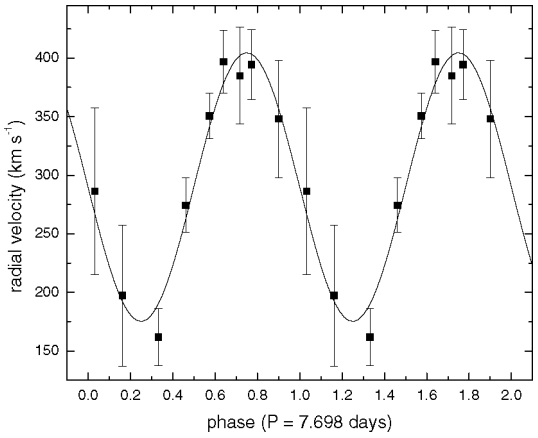

Figure 7. OGLE 05060009–6855025 radial velocities folded with twice the short photometric period. For best visualization, we show the average of the RVs per phase bin, along with its standard deviation as error bars.

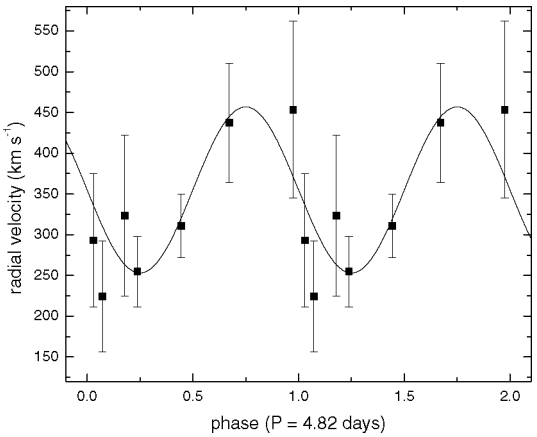

Figure 8. Same as in Fig. 7 for OGLE 05195898-6917013.

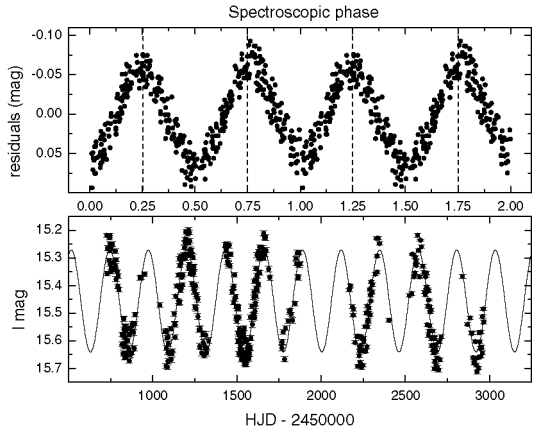

Figure 9. The bottom panel shows the long-term OGLE light curve for OGLE 05060009-6855025 and the best sinus fit. The upper panel shows the residuals of this fit folded with the spectroscopic ephemeris.

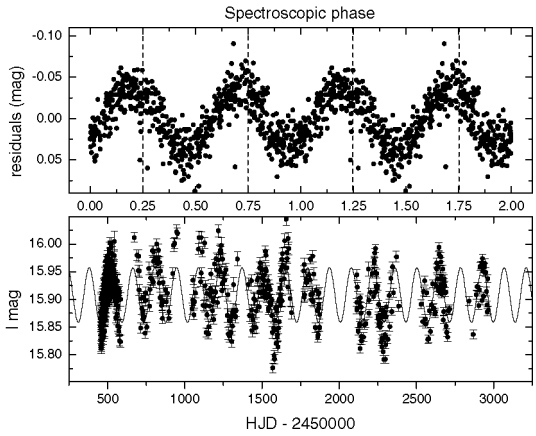

Figure 10. Same as in Fig. 9 for OGLE 05195898-6917013.

In addition, to allow disc formation, the so-called circularization radius $Rr_{\rm circ}$ should be larger than the radius of the mass-gaining star. The circularization radius for Roche lobe overflow is given by

$$R_{\rm circ} \cong 4(1+q)^{4/3}\,(0.500 - 0.227\log q)^4\,P^{2/3}\,{\rm R}_\odot \qquad (3)$$

(Frank, King & Raine 2002). For an orbital period of 5 d this formula yields a circularization radius of between 5 and 1.6 $\rm R_\odot$ for $0.05 \leqslant q \leqslant 10$. The corresponding figures for a binary with an orbital period of 18 d are 11.5 and 3.7 $\rm R_\odot$, respectively. Therefore, we conclude that if the hypothesis of disc formation is correct, the mass-gaining star could be a dwarf or even a white dwarf with an accretion disc, although an evolved star of spectral type roughly between B5 and G5 would also fit inside its Roche lobe and even allow some space for disc formation. We discard the massive X-ray binary hypothesis on the basis of a lack of X-ray emission. A crosscheck of the targets in the NASA HEASARC (http://heasarc.gsfc.nasa.gov/) reveals only a couple of low-probability associations with *ROSAT*, *XMM* or *Chandra* sources.

The observation of the colour–magnitude (CM) diagram for the LMC double-periodic variables reported by M03 along with the three new objects reported earlier in this paper (Fig. 11) shows that these systems have colours and magnitudes consistent with an evolved, rather giant but not supergiant, B-A type star. The three SMC double-periodic blue stars reported by M03 occupy basically the same position regarding the SMC main sequence. Interestingly,

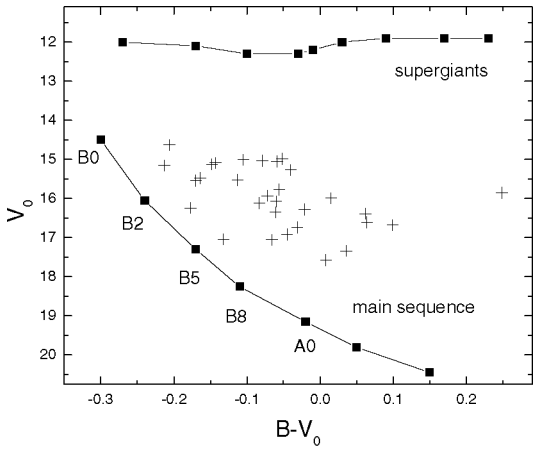

Figure 11. The dereddened colour–magnitude diagram for the double-periodic stars in the LMC reported by M03. Three new stars documented in Section 3.1 are also plotted. We show the main-sequence and supergiant location based on Cox (2000) data and using an LMC distance module of 18.5. Errors of the OGLE photometry are typically less than 0.02 mag. From this diagram we conclude that most systems are likely evolved. Reddening values for each star were taken from Udalski et al. (1999).

this is consistent with the expectation for the donor obtained through equation (1) and with the BCD classification given in Section 3.2 for most objects studied spectroscopically in this paper.

We conclude that spectroscopy supports, in principle, the scenario of semidetached binaries for double-periodic variables with the donor star as the primary, brighter component.

4.2 On the nature of the cooler component and system parameters

In the case that the short-term variability observed in the light curves of double-periodic variables are the ellipsoidal variations of the brighter component, we could combine the dynamical information obtained from the radial velocity analysis of OGLE 05060009-6855025 and OGLE 05195898-6917013 with the photometric amplitudes of its short-term variations in order to obtain constraints on the system inclination and the mass ratio.

An expression for the full amplitude of the ellipsoidal variations is given by:

$$\Delta m({\rm mag}) \approx \frac{3}{2q} f^3 (R/a)^3 \sin^2 i (1+\tau_0)\frac{15+u}{15-5u} \qquad (4)$$

(Russell 1945; McClintock et al. 1983), where f is the radial fraction of the Roche lobe which is filled, i is the systemic inclination angle and R/a is the ratio of the Roche lobe radius of the donor star to the distance between the stars. τ_0 and u are the gravity-darkening and limb-darkening coefficients, respectively.

On the other hand, the mass function can be written as

$$\frac{PK_2^3}{2\pi G} = \frac{M_2 \sin^3 i}{q(1+q)^2}, \qquad (5)$$

where K_2 and M_2 are the radial velocity half-amplitude and mass of the donor star, respectively. We can combine both equations in order to obtain an expression for the mass ratio eliminating $\sin i$. Using $R/a \approx 0.38 + 0.20\log q$, which is accurate to 2 per cent in the range $0.3 < q < 20$ (Paczyński 1971), we obtain

$$\frac{(1+q)^2(0.38+0.20\log q)^{9/2}}{\sqrt{q}} = \frac{\Delta m^{3/2} M_2 C}{P(K_2/213)^3}, \qquad (6)$$

where M_2 is in solar masses, P is in d, K is in km s^{-1} and C is a constant given by

$$C = \left[\frac{2}{3f^3}\frac{(15-5u)}{(1+\tau_0)(15+u)}\right]^{3/2}. \quad (7)$$

For OGLE 05060009-6855025 and OGLE 05195898-6917013 limb-darkening coefficients of 0.22 and 0.21 were obtained from Al-Naimiy (1978), who provide a grid of limb-darkening coefficients, calculated from model atmospheres, as a function of effective temperature, wavelength and gravities. These values are corroborated by modern limb-darkening coefficients based on ATLAS stellar atmosphere models (van Hamme 1993). For the gravity-darkening coefficient we used the value of 1, for a star where the subsurface layers transfer energy uniquely by radiation (von Zeipel 1924), but this parameter could be larger even by 50 per cent in highly distorted hot stars filling their Roche lobes in semidetached binaries (Djurašević et al. 2003). The factor f was assumed to be equal to 1. The full amplitude of the ellipsoidal variations were calculated by fitting a sinus function to the long-term residuals phased with the short period. These amplitudes resulted in 0.120(1) and 0.072(2) for the I-band light curves of OGLE 05060009-6855025 and OGLE 05195898-6917013, respectively. We also measured these amplitudes for the $b-r$ MACHO light curves (freely available at http://wwwmacho.mcmaster.ca/), obtaining 0.122(1) and 0.128(2) for the b and r OGLE 05060009-6855025 light curves and 0.078(1) and 0.080(1) for the b and r OGLE 05195898-6917013 light curves. The fact that the amplitude of the short-term variability in these stars is practically independent of wavelength suggests that the secondary star has a neglectable contribution to the system light over a wide wavelength range. We therefore assume that these amplitudes correspond to the full light amplitude of the primary and we have used these values as Δm in equation (6).

Using equation (6) and assuming $M_2 = 7$ M$_\odot$, representative for a B5 III star, we find $q = 0.85 \pm 0.11$ for OGLE 05060009-6855025 and q between 0.55 and 1.60 for OGLE 05195898-6917013 with the most likely value being 0.9. The errors above consider only the uncertainty in the more sensitive parameter K. Underestimating τ_0 by 50 per cent decreases q down to 0.7 in OGLE 05060009-6855025 and up to 0.7 in OGLE 05195898-6917013, whereas an uncertainty of 20 per cent in M_2 yields to an error of 13 per cent in q. On the other hand, the underfilling of the Roche lobe by 10 per cent ($f = 0.9$) increases the mass ratio by 36 per cent. The most likely inclination compatible with the quantities derived above for OGLE 05060009-6855025 is $53° \pm 8°$, whereas for OGLE 05195898-6917013 the uncertainties in q and K are too large to provide a reasonable inclination estimate. Our estimates above suggest that the second component should have a mass of between 6 and 10 M$_\odot$ for OGLE 05060009-6855025 and OGLE 05195898-6917013. This should correspond to an early B-type star. If the radial velocities are not heavily contaminated by an emission source, and reflect the orbital motion of the brighter component, then the possibility of a white dwarf secondary is excluded by the dynamical solution in both systems. In addition, the almost zero contribution to the radiative flux of the secondary star in both systems should indicate a dwarf rather a giant. The circularization radius given by equation (3) is 2.5 R$_\odot$ for OGLE 05060009-6855025 and 1.9 R$_\odot$ for OGLE 05195898-6917013. This means that disc formation by accretion of material from the primary star is not possible for secondaries fitting the dynamical solution (typical radii for early B-type dwarfs are 7–4 R$_\odot$). Another cause besides emission from an accretion disc around the secondary should be invoked to explain the filling by emission of the Balmer absorption lines in these systems.

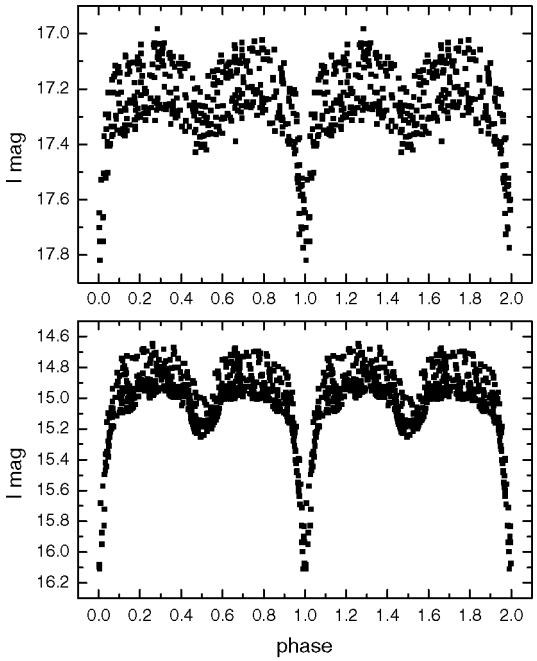

Figure 12. The light curves of OGLE 05052263-6852002 (up) and OGLE 05200407-6936391 (down) folded with the respective short-term periods. No pre-whitening has been applied in these cases. The vanishing of the long-term variability (noisy pattern) during the main eclipses indicates an origin of this variability in the brighter component.

Our finding above contradicts the hypothesis outlined by M03 that the long-term photometric variability could be due to precession of an elliptical accretion disc in a low-mass ratio semidetached binary. If disc precession is excluded as an explanation, there must be another cause for the long-term variability.

4.3 On the nature of the long-term variability and the pulsation hypothesis

Fig. 12 shows the light curves of OGLE 05052263-6852002 and OGLE 05200407-6936391 folded with their short-term periods. The remarkable fact in these figures is the vanishing of the long-term variability during the main eclipse. A similar behaviour is observed in all the eclipsing binaries reported by M03; the long-term oscillation always disappears at the main minimum but it is present, sometimes with lower amplitude, in the secondary minimum. This can only be interpreted if the main origin of the long-term variations is the brighter star.

We have explored the possibility that the photometric variability in the non-eclipsing DPVs could reflect a beat phenomenon in multiperiodic pulsating stars. This idea arises from the fact that the long-term periods are also very typical for beat periods of non-radial gravity mode oscillations in B-type stars, the so-called slowly pulsating B stars (hereafter SPBs, e.g. Waelkens 1991; De Cat & Aerts 2002). Moreover, De Cat et al. (2000) have shown the case of HD 92287, a single line B-type binary with a circular orbit showing ellipsoidal variations and g-mode pulsations which are easily mixed up in single-band photometry. On the other hand, the position of the target stars in the colour–magnitude diagram (Fig. 11) is very similar to those of a sample of periodically variable B-type supergiants found by Waelkens et al. (1998) from the *Hipparcos* mission.

The pulsation hypothesis is particularly relevant now that pulsating B stars have been found in the Magellanic Clouds (Kolaczkowski et al. 2004).

We cannot directly test the presence of very short periods in our sample of DPVs, due to the sampling of the OGLE-MACHO data. In the future we plan to do that, monitoring our targets with higher time resolution. At the moment, the Nyquist frequency is approximately 0.5 c d^{-1} in most cases. However, we can check for the presence of periodicities larger than 2 d. For that we have pre-whitened the light curves shown in Fig. 12 with the binary solution. The binary light curve was obtained by fitting the data with a double sinusoid excluding the main minimum. Residuals to this fit were analysed searching for multiple periods. No trace of additional periodicities were found apart from the fundamental frequency of the long-term oscillation. For that, and for the following reasons we believe that the pulsation hypothesis based on SPBs or α-Cyg-type pulsations is incompatible with the data. (i) The amplitude of the long-term variations is almost constant in most cases, this is not the usual case for stars showing the phenomenon of beating of multiple oscillations. (ii) The amplitude of the long-term variability is rather large (approximately 0.2 mag) when compared with the amplitude of SPBs (approximately 0.02 mag) or even with amplitudes of α-Cyg-type supergiants (<0.1 mag) and it is hard to image how a beat of low-amplitude oscillations could produce the observed large-amplitude variability. (iii) There is no colour dependence in the short-term variability of DPVs, contrary to the pulsations observed in SPBs. (iv) The long-term oscillations are red, contrary to the SPBs pulsations which are blue. (v) The periodogram of SPBs looks completely different from the periodograms of DPVs; they clearly show the presence of multiple periods in the range of 1–3 d, and no presence of a long periodicity over 100 d. In contrast, periodograms of DPVs shows a strong minimum at the long period (indicating a fundamental frequency) and no evidence for multiple periods in the short-period range, except for the short-term periodicity that always appears with much less power than the longer one. (vi) Concerning α-Cyg-type supergiants, such as those found by Waelkens et al. (1998), they show multiple periods, and their light curves are highly irregular in shape, and include the presence of microvariability; they do not show the strictly periodic pattern of DPVs characterized by a single short period.

Although the above points argue against SPBs-type or α-Cyg-type pulsations, we cannot exclude the presence of very short pulsations of a new nature in these objects, and defer this question for future photometric studies with higher time resolution.

4.4 On the importance of stellar winds and mass-loss rates

It is well known that early B-type giants have significant mass-loss rates due to radiatively driven winds (e.g. Vink, de Koter & Lamers 2001). In addition, it has been shown that near-critical rotation could induce extreme mass loss in massive stars even far from the Eddington limit (Aerts, Lamers & Molenberghs 2004). Following these arguments we have explored the possibility that the weakness of the Hβ line could be due to mass loss in some of the DPVs.

In the following, we assume the contribution of the less luminous star and any other light source to be neglectable to the overall light of the system. Hence the derived parameters refer to the primary, the more luminous star. We estimated $V \sin i$ from the full linewidths of the He I 4471 and Mg II 4481 lines. Errors are of the order of 40 km s^{-1}, a large value mainly due to the low resolution of our spectra. The results, shown in Table 8, indicate that the stars are rotating with higher velocities than those obtained by assuming corotation with the binary system. The stellar masses derived according to $M_{\rm bol}$ (Table 4) and using the Maeder & Meynet (1988), Maeder & Meynet (1989) evolutionary tracks are also shown in Table 8, along with the stellar radius, calculated from the $\log g$ values. The mass-loss rates given in Table 8 are derived from Vink et al. (2001), assuming $Z_{\rm LMC} = 1.0$ and $Z_{\rm SMC} = 0.1$. The $V \sin i$ values indicate that the stars are rotating at a large fraction of the critical velocity (Table 8, column 5). On the other hand, the stars are far from the Eddington limit (Table 8, column 6). Applying the recipe given by Aerts et al. (2004) for mass-loss rates of rotating massive stars, we found that the rotational contributions to the total mass-loss rates are less than $\log \dot{M} = 0.02$ and therefore neglectable for our objects. Looking at the $\dot{M}$ values we find that they are comparable to the $\dot{M}$ values observed in Be stars in the polar regions. We attribute the large $\dot{M}$ value of OGLE 05410942-7002215 to the doubtful spectral classification for this star, as this extreme mass-loss rate does not correspond with the rather 'normal' spectral appearance of OGLE 05410942-7002215 in Fig. 6. Be stars show low-density stellar winds in the poles, which are usually detected in UV resonance lines, so the calculated $\dot{M}$ values cannot explain the filling by emission observed in DPVs.

4.5 A link with Be stars?

The fact that the primaries in DPVs seem to be fast rotators raises the question of whether or not they are Be stars. Be stars have, apart from their polar winds, circumstellar disc-like envelopes in the equatorial regions, which could explain the weakness of the Hβ line by filling by emission from an optically thin gas envelope. An optically thin, low-temperature envelope should produce an emission line pattern with a steep Balmer decrement, which would be observed as selective filling-up; larger amounts of emission should be observed in lower-order Balmer lines, as apparently occurs. The contribution to the continuum by an optically thin envelope could be negligibly small at optical wavelengths. If the above picture is

Table 8. $V \sin i$ estimates based on the width of the He I 4471 and Mg II 4481 lines. We also show the stellar mass, equatorial radius, lower limit for the ratio between the rotational velocity and the critical velocity $v/v_{\rm c}$, the ratio Γ between the luminosity and the Eddington luminosity and the mass-loss rate $\dot{M}$ by radiation-driven winds. The ratio f between the primary radius and their Roche lobe volume radius, assuming B-type dwarf secondaries, is also given.

Star	$V \sin i$ (km s^{-1}) or note	M ($M_\odot$)	R ($M_\odot$)	$v/v_{\rm c}$	Γ	$\dot{M}(M_\odot\ {\rm yr}^{-1})$	f
OGLE 00451755-7323436	Noisy	11	6.5	NA	0.04	−10.7	0.5
OGLE 00553643-7313019	270	11	4.1	0.46	0.04	−11.7	0.3
OGLE 05060009-6855025	240	7	16.4	1.03	0.02	−11.0	1.1
OGLE 05155332-6925581	140	5.5	12.1	0.58	0.01	−11.2	0.9
OGLE 05195898-6917013	180	5.5	7.2	0.58	0.01	−11.2	0.7
OGLE 05313130-7012584	>300	7	9.8	1.00	0.02	−10.8	0.5
OGLE 05410942-7002215	Noisy	14	22.0	NA	0.08	−9.1	1.2

true, future observations of the Hα line or the IR continuum should reveal the emitting envelope unambiguously.

In order to check the possibility that the long-term variability arises from a disc-like envelope around a Be-star primary, we calculated if there is enough room for a disc around the primary star. Using classical formulae for close binary systems (e.g. Warner 1995), and assuming a secondary mass compatible with a B spectral type, we estimated the fraction of the Roche lobe filled by the brighter component (the f factor defined in Section 4.2). This factor depends on the stellar masses, orbital period and primary radius. Its uncertainty is mainly determined by errors in the primary mass and radius. We estimated errors for $f \sim 10$ per cent for $f \approx 1$ and $\sim$50 per cent for $f \approx 0.3$. From the f values given in Table 8, we conclude that nearly half of the systems have room for a disc, just a very small disc. On the other hand, OGLE 05060009-6855025, OGLE 05155332-6925581 and OGLE 05410942-7002215 have primaries filling or nearly filling their Roche lobes. It is interesting to note that systems with more room for a disc, OGLE 00451755-7323436 and OGLE 00553643-7313019 ($f = 0.5$ and 0.3, respectively), are those with larger Hβ emission (in fact, the line is almost absent in their spectra, see Fig. 6). OGLE 05313130-7012584, on the other hand, also has a low-f value (equal to 0.5), but this star shows no special Hβ filling. We conclude that very small gaseous discs are possible around the primaries of only some DPVs, and that some other systems are candidates for semidetached binaries. For this reason the putative discs are probably not the source of the long-term variability.

5 CONCLUSIONS

Evidently, we do not have the complete solution for the DPVs at this moment. Our findings support the hypothesis that these objects are close binary systems consisting of B type primaries and secondaries. We identify the shorter periodicity in non-eclipsing systems as the ellipsoidal variation of the brighter component which fills a considerable fraction of their Roche lobe. A problem which remains to be solved refers to the origin of the long-term photometric period in these systems. We have identified the source of this variability in or around the primary star. We do not know if it implies a new kind of stellar pulsation. In this regard, high time resolution photometry is highly desirable, as it could provide insights concerning the pulsation properties of these stars. Further spectroscopic studies, especially in the infrared, are also necessary to investigate the nature of the long-term variation, the cooler companion and the peculiar intrinsic colour excesses. We need to understand how these binary systems evolve and how their evolution depends on mass, mass exchange and chemical content.

The main conclusions of the analyses reported in the previous sections can be summarized as follows.

(i) Spectra of seven double-periodic blue variables are consistent with B-type stars of luminosity class between IV and III.

(ii) Radial velocity variations of the Hβ absorption line reveal the binary nature of OGLE 05060009-6855025 and OGLE 05195898-6917013.

(iii) In these cases the short-term periodicities are consistent with ellipsoidal variations of the brighter component.

(iv) The large fraction of eclipsing binaries (six cases) found in the whole sample of 33 double-periodic variables suggests that the probability of identifying this kind of variable depends on the system inclination being larger for high-inclination systems.

(v) We suspect that some of the type 3 stars (i.e. those showing long-term periodicities) reported by M02 and not classified as double-periodic variables are the same kind of system but seen at lower inclination. This is consistent with the interpretation of the short-term photometric modulation as ellipsoidal variations of the brighter component.

(vi) The dynamical solution and the analysis of the short-term light curve of these objects indicate a mass for the cooler companion between 6 and 10 $M_{\odot}$. This means early B-type secondaries, excluding the possibility for accretion disc formation around them.

(vii) Estimates of the companion temperature based on the light-curve analysis indicate that they are lower by factors of 0.8–0.9 than those of the hotter components. This finding is compatible with B-type companions and with the absence of significant colour variations during the orbital cycle.

(viii) A study of the rotational velocities of the brighter components indicate rotational velocities larger than that expected for synchronization with the binary orbit. This opens the possibility for Be-type primaries.

(ix) We find the long-term variability practically disappears during the main eclipse in the eclipsing DPVs. This means that the origin of the long-term variability is in or around the primary star.

(x) No known pulsation mechanism can explain the long-term variations. The presence of very short pulsations of a new nature in the primary star cannot be discarded with the present data.

(xi) The origin of the apparent filling of the absorption lines and the flatness of some continua could be due to free–free and free–bound emission from a cool circumstellar envelope, but this needs to be confirmed with infrared spectroscopy.

ACKNOWLEDGMENTS

We acknowledge useful insights provided by the referee, Conny Aerts, which helped to improve the scientific discussion in this paper, especially concerning the hypothesis of stellar pulsations. RM acknowledges support by Fondecyt grant 1030707. RM, WG and GP acknowledge support from the Chilean FONDAP Centre for Astrophysics 15010003. BS acknowledges support by Programa MECE Educación Superior UCO0209.

REFERENCES

Aerts C., Lamers H. J. G. L. M., Molenberghs G., 2004, A&A, 418, 639
Al-Naimiy H. M., 1978, Ap&SS, 53, 181
Barbier D., Chalonge D., 1941, Ann. Astrophys., 4, 30
Chalonge D., Divan L., 1952, Ann. Astrophys., 15, 201
Cidale L., Zorec J., Tringaniello L., 2001, A&A, 368, 160
Collins G. W., Truax R. J., Cranmer S. R., 1991, ApJS, 77, 541
Cox A. N., 2000, Allen's Astrophysical Quantities. Springer-Verlag, New York
De Cat P., Aerts C., 2002, A&A, 393, 965
De Cat P., Aerts C., De Ridder J., Kolenberg K., Meeus G., Decin L., 2000, A&A, 355, 1015
Didelon P., 1982, A&AS, 50, 199
Divan L., Zorec J., 1982, ESA-SP, 177
Djurašević G., Rovithis-Livaniou H., Rovithis P., Georgiades N., Erkapić S., Pavlović R., 2003, A&A, 402, 667
Eggleton P. P., 1983, ApJ, 268, 368
Flower P. J., 1977, A&A, 54, 31
Frank J., King A., Raine D. J., 2002, in J. Frank, A. King, D. J. Raine, eds, Accretion Power in Astrophysics, 3rd edn. Cambridge Univ. Press, Cambridge

Kolaczkowski Z. et al., 2004, in D. W. Kurtz, K. R. Pollard, eds, IAU Colloq. 193, ASP Conf. Proc. Vol. 310, Conf. Variable Stars in the Local Group. Astron. Soc. Pac., San Francisco, p. 225
McClintock J. E., Petro L. D., Remillard R. A., Ricker G. R., 1983, ApJ, 266, L27
Maeder A., Meynet G., 1988, A&AS, 76, 411
Maeder A., Meynet G., 1989, A&A, 210, 155
Mennickent R. E., Pietrzyński G., Gieren W., Szewczyk O., 2002, A&A, 393, 887 (M02)
Mennickent R. E., Pietrzyński G., Diaz M., Gieren W., 2003, A&A, 399, L47 (M03)
Mennickent R. E., Assmann P., Pietrzyński G., Gieren W., 2004, in Sterken C., ed., ASP Conf. Ser. Vol. 335, Proc. Workshop The Light-Time Effect in Astrophysics. Astron. Soc. Pac., San Francisco, p. 129
Paczyński B., 1971, ARA&A, 9, 183
Russell H. N., 1945, ApJ, 102, 1
Slettebak A., 1985, ApJS, 59, 769
Udalski A., Szymanski M., Kubiak M., Pietrzynski G., Wozniak P., Zebrun K., 1998, Acta Astron., 48, 147
Udalski A., Soszynski I., Szymanski M., Kubiak M., Pietrzynski G., Wozniak P., Zebrun K., 1999, Acta Astron., 49, 223
van Hamme W., 1993, AJ, 106, 2096
Vink J. S., de Koter A., Lamers H. J. G. L. M., 2001, A&A, 369, 574
von Zeipel H., 1924, MNRAS, 84, 702
Waelkens C., 1991, A&A, 246, 453
Waelkens C., Aerts C., Kestens E., Grenon M., Eyer L., 1998, A&A, 330, 215
Warner B., 1995, Cataclysmic Variable Stars, Cambridge Astrophysical Series 28. Cambridge Univ. Press, Cambridge
Welch D. L., Cote P., Fischer P., Mateo M., Madore B. F., 1991, AJ, 101, 490
Zebrun K. et al., 2001, Acta Astron., 51, 317
Zorec J., 1986, PhD thesis, Paris Universite VII
Zorec J., Briot D., 1991, A&A, 245, 150

This paper has been typeset from a TEX/LATEX file prepared by the author.